Bansode Balbhim Narhari*, Bakwad Kamlakar Murlidhar, Ajij Dildar Sayyad and Ganesh Shahubha Sable

Automated diagnosis of diabetic retinopathy enabled by optimized thresholding-based blood vessel segmentation and hybrid classifier

https://doi.org/10.1515/bams-2020-0053
Received September 10, 2020; accepted November 2, 2020; published online

Abstract

Objectives: The focus of this paper is to introduce an automated early Diabetic Retinopathy (DR) detection scheme from colour fundus images through enhanced segmentation and classification strategies by analyzing blood vessels.

Methods: The occurrence of DR is increasing from the past years, impacting the eyes due to a sudden rise in the glucose level of blood. All over the world, half of the people who are under age 70 are severely suffered from diabetes. The patients who are affected by DR will lose their vision during the absence of early recognition of DR and appropriate treatment. To decrease the growth and occurrence of loss of vision, the early detection and timely treatment of DR are desirable. At present, deep learning models have presented better performance using retinal images for DR detection. In this work, the input retinal fundus images are initially subjected to pre-processing that undergoes contrast enhancement by Contrast Limited Adaptive Histogram Equalization (CLAHE) and average filtering. Further, the optimized binary thresholding-based segmentation is done for blood vessel segmentation. For the segmented image, Tri-level Discrete Level Decomposition (Tri-DWT) is performed to decompose it. In the feature extraction phase, Local Binary Pattern (LBP), and

*Corresponding author: Bansode Balbhim Narhari, Research Scholar, Department of Electronics & Telecommunication Engineering, MIT College of Engineering, Dr. Babasaheb Ambedkar Marathwada University, Aurangabad, India,

E-mail: bansodebalbhim78@gmail.com

Bakwad Kamlakar Murlidhar, Department of Electronics Engineering, Puranmal Lahoti Govt. Polytechnic College, MSBTE, Latur, Mumbai, India

Ajij Dildar Sayyad and Ganesh Shahubha Sable, Department of Electronics & Telecommunication Engineering, MIT College of Engineering, Dr. Babasaheb Ambedkar Marathwada University, Aurangabad, India

Gray-Level Co-occurrence Matrices (GLCMs) are extracted. Next, the classification of images is done through the combination of two algorithms, one is Neural Network (NN), and the other Convolutional Neural Network (CNN). The extracted features are subjected to NN, and the tri-DWT-based segmented image is subjected to CNN. Both the segmentation and classification phases are enhanced by the improved meta-heuristic algorithm called Fitness Ratebased Crow Search Algorithm (FR-CSA), in which few parameters are optimized for attaining maximum detection accuracy.

Results: The proposed DR detection model was implemented in MATLAB 2018a, and the analysis was done using three datasets, HRF, Messidor, and DIARETDB.

Conclusions: The developed FR-CSA algorithm has the best detection accuracy in diagnosing DR.

Keywords: average filtering; contrast limited adaptive histogram equalization; convolutional neural network; diabetic retinopathy; fitness rate-based crow search algorithm; gray-level co-occurrence matrices; neural network; optimized binary thresholding; tri-level discrete level decomposition.

Introduction

Diabetic Retinopathy (DR) is the disease, which is usually seen in diabetic patients associated with the damage of retina caused due to diabetes mellitus that lives a long time [1, 2]. The major cause of DR is the loss of vision and blindness as it is traced globally to "2.6 million cases" of huge vision deficiency and "0.4 million cases" of blindness in the year 2015. If the disease is detected and treated in time, the abnormality of DR to vision can be prevented or avoided. However, as there are some symptoms in the early stage of DR, several patients might miss the best time for treating DR. Moreover, DR detection has extremely relied on the analysis and observation of fundus images and this process will consume more amount of time even for the experts.

By using highly trained domain experts, manual analysis has been performed and thus it is expensive when

computing time and costs are considered. For evaluating the fundus images automatically, it is significant for using computer vision models, which helps the radiologists or physicians. The approaches based on computer vision are split into "end-to-end learning [3-5] and hand-on engineering" [6-8]. The hidden rich features are learned by end-to-end learning automatically and therefore better classification is done. By using conventional models like Gabor filters [9], HoG [10], LBP [11], and SIFT [12], the handon-engineering models will extract the features and it fails to encode the illumination, rotation and scale variations. To detect DR in Kaggle dataset, numerous "end-toend and hand-on engineering-based techniques" [13-15] are employed; still, there is no method for mild stage detection. This stage detection is significant for early control. To detect DR accurately, CAD models have more possibilities in less span of time that will assist the physician further for decreasing the count of blindness and enhancing the DR screening rate [16].

Several approaches have been introduced in the past 20 years to detect DR automatically. By many techniques, a typical model is used for particular DR lesion detection prior to the diagnosis of the entire retinal fundus image [17]. In general, to categorize the image patches as abnormal and normal, supervised learning models are applied. This kind of approaches is based on DR lesion manual annotation that leads to cause more workload to the clinicians over retinal image DR gradation. As a result, the generation of the training dataset is obstructed, in which the data-driven models are learned in a better way for dealing with discrete conditions of DR. A weakly supervised learning model called MIL [9] was analyzed by various researchers for saving the annotation cost and to learn, more retinal images are made available [18, 19]. To classify the image patches, the models that are introduced until now make use of the handcrafted features. By using MIL, the authors failed to attain advantages from vast datasets that are frequently producing less detection accuracy over other supervised learning techniques.

The major contribution of the implemented DR detection technique is shown below.

- To introduce a new method for detecting DR by considering the input fundus images using an effective segmentation and classification algorithm.
- To maximize the detection accuracy by introducing an improved meta-heuristic algorithm that optimizes the relevant parameters.
- To perform accurate blood vessel segmentation using optimized binary thresholding that could segment the blood vessels with high accuracy.

- To decompose the blood vessel segmented image with a decomposition model named Tri-DWT, and to extract a set of features using GLCM and LBP for classifying the images.
- To classify the images by the combination of NN and CNN, in which the extracted features are subjected to NN and the decomposed image are subjected to CNN and the count of hidden neurons are tuned by the improved FR-CSA algorithm.

The entire paper is modeled as: Section 2 represents the review of existing DR detection models. In Section 3, DR diagnosis from retinal fundus images is discussed. The optimal binary thresholding-based blood vessel segmentation with feature extraction is shown in Section 4. In Section 5, the FR-CSA for optimal blood vessel segmentation and detection is shown. The results and discussions of the entire paper are given in Section 6. The final Section 7 shows the conclusion of the paper.

Literature review

Related works

In 2018, Costa et al. [20] have recommended a new technique based on the MIL approach for surpassing the requirement by leveraging the implicit data existing on the annotations made in the image level. Many helpful midlevel depictions of pathological images were acquired in such a manner. Further, the suggested model's explainability was improved by applying a new loss function with mid-level depictions and suitable instance. The developed approach attained the best performance when compared to other approaches.

In 2018, Kar and Maity [21] have introduced a new and automatic lesion detection model. To provide further processing, the suppression of optic disc and blood vessels was done. For separating the dark lesions, Curvelet-based edge improvement was performed. The wideband bandpass filter was improved when the brightness among the background and bright lesions. Later, the mutual information of the maximum Laplacian of Gaussian response and matched filter response were combinedly maximized. To determine the optimal values for the parameters of fuzzy functions, a differential evolution algorithm was employed, which defined the segmentation thresholds of the candidate regions. For removing the false detection of candidate pixels, morphology-based post-processing was applied.

In 2018, Zhou et al. [22] have developed the MIL technique for detecting DR that together learned the features as

well as classifiers from the data and attained a more improvement in DR image and its lesion detection. To attain the patch-level DR estimation, a pre-trained CNN was employed. Later, for performing the DR image classification, global aggregation was employed. To tackle with irregular DR lesions, the researchers introduced an end-to-end multi-scale model. By using two datasets named Kaggle and Messidor, the proposed model was analyzed.

In 2018, Amin et al. [23] have applied an automatic approach for DR detection and classification. For enhancing the region of interest, a local contrast enhancement approach was utilized. For precise lesion segmentation, an adaptive threshold approach by mathematical morphology was employed. Next, to perform better classification, both statistical and geometrical features were combined. The datasets such as E-ophtha, DIA-RETDB1, local datasets and Messidor datasets were used for validating the developed model using various measures like accuracy and area under the curve.

In 2018, Xu et al. [24] have developed an innovative algorithm that included two procedures from pathological risk factors, and microaneurysms turnover for detecting the growth of DR. To acquire the turnover of microaneurysms, one method followed a conventional image analysis-based roadmap. For classifying the resolved microaneurysms, new and unchanged with the pattern classification and statistical analysis approaches, the other analyzed seven pathological features associated with the turnover microaneurysms. The developed model was evaluated on the "Grampian diabetes database". It has shown that the model attained huge specificity and sensitivity.

In 2019, Zheng et al. [1] have suggested a CAD model based on deep learning techniques for diagnosing referable DR automatically by categorizing color fundus images into normal and abnormal. CNN using a Siamese-like structure was trained by the transfer learning approach. The developed method allowed binocular retinal images as inputs and learned their correlation for assisting to make the prediction. The outcomes have shown that it attained the best kappa score that was more when compared over non-ensemble approaches.

In 2019, Qummar et al. [8] have been suggested discrete computer vision-based models for both DR and its various stages of detection from retinal images. However, these techniques were not able to encode the basic complex functions and have the ability to categorize various stages of DR by attaining less accuracy especially in the early stages of detection. To train deep CNN approaches like "Dense121, Xception, Dense169, Resnet50, and

Inceptionv3" for encoding the rich features and the enhancement of discrete DR stages classification, freely accessible Kaggle dataset related to retinal images. The outcomes have revealed that the developed approach detected all DR stages when compared to traditional approaches.

In 2020, Roshini et al. [25] have introduced an automated DR detection scheme. In pre-processing, the conversion of RGB to lab and histogram equalization was done. The segmentation process includes three steps for attaining the segmented images. The adaptive average filtering process was used for filtering, and the filter coefficients were tuned using an enhanced heuristic algorithm named FP-CSO. The classification was performed by Deep CNN, in which the enhancement was done on the convolutional layer that was optimally tuned using the proposed FP-CSO algorithm.

Review

Although there are many benefits with the existing DR detection models, still there are few conflicts with those models so that an effective model needs to be implemented for DR detection. Some of the pros and cons of the existing DR detection models are tabulated in Table 1.

Diabetic retinopathy diagnosis from retinal fundus images

Developed architecture

In all over the world, DM has significant morbidity and mortality, which are usually seen in not only in huge developed countries but also in developing countries. The effect of DM causes a specific challenge to the healthcare systems in several developing countries. DR consists of some microvascular complications, which becomes severe for time. The different stages of DR are PDR and DME that in turn cause blindness and visual impairment. For diagnosing both DME and PDR, there are efficient and high computational cost treatments. The diagrammatic representation of the proposed DR detection model is shown in Figure 1.

The proposed DR detection model concerning color fundus images perform enhanced segmentation and classification mechanisms by evaluating blood vessels. The developed method includes "pre-processing, blood vessel

Table 1: Review of existing diabetic retinopathy detection models.

Author [citation]	Methodology	Features	It doesn't encode the position and orienta- tion of an object. It requires the spatial invariance of the input data.	
Zeng et al. [1]	CNN	 It has attained the best kappa score. It is used for the automatic detection of RDR. 	•	
Qummar et al. [8]	Deep CNN	 It is used for rich feature encoding and enhances the classification performance for various DR phases. It has attained the best performance. 	 It requires the spatial invariance of the input data. 	
Costa et al. [20]	MIL	 It is used to classify the bags into two classes. It efficiently uses the local information present on the image to a similar level. 	 If the instances don't have accurate classes, it won't work well. 	
Kar and Maity [21]	DE	 It is used to define the optimal values for the fuzzy function parameters. It has the best detection accuracy. 	 It has an unstable convergence in the last period and can easily fall into local optima. 	
Zhou et al. [22]	Deep MIL	 It attains an improved performance in DR images and their lesion detection. the performance is improved by acquiring the efficiency of feature learning. 	- It is less accurate.	
Amin et al. [23]	Ensemble bag- ged tree	 It has attained the best performance when compared to other classifiers. It ensures the stability of the model. 	 It has an over-fitting problem. 	
Roshini et al. [25]	Deep CNN	 It is used to classify the severity of exactness. It produces good reliability and validity and is strong for data variations. 	- It is computationally expensive.	
Xu et al. [24]	SVM	 It has a specific indication to find the feature weights. It is found to be more effective for classification problems. 	 It is not suitable for vast datasets. 	

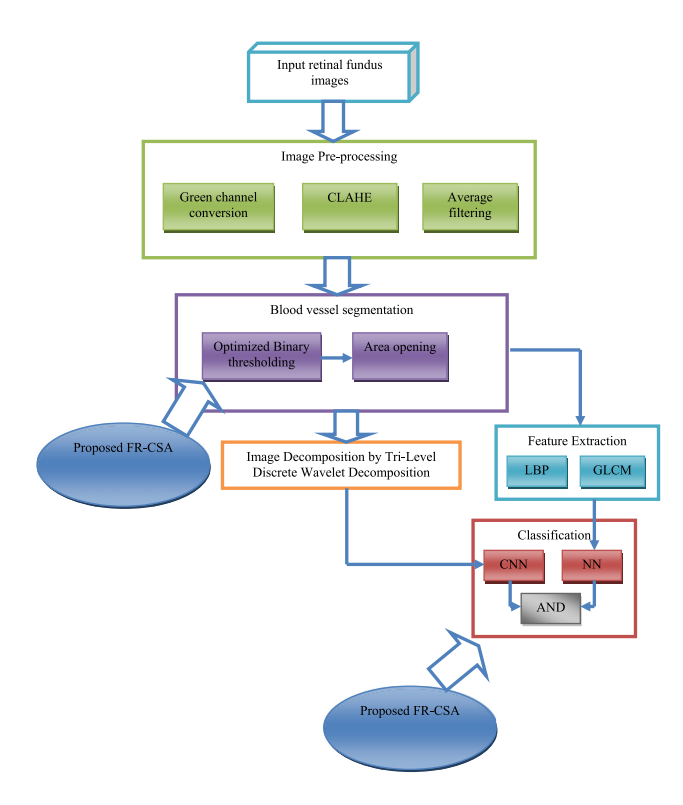


Figure 1: Proposed architecture of DR detection model.

segmentation, image decomposition, feature extraction and classification". Initially, the input retinal images are given to the pre-processing phase, in which green channel conversion, CLAHE, and average filtering methods are done. While performing CLAHE operation, the visibility of the image is improved, whereas average filtering performs the smoothing of the image by minimizing the amount of intensity between the pixels. Next, the blood vessel segmentation is done by optimized binary thresholding using FR-CSA, and area opening. To decompose the blood vessel segmented image, Tri-DWT is used. Once the segmentation is performed, the features such as LBP and GLCM features are extracted from the blood vessel segmented images. These features are subjected to the machine learning algorithm named NN, whereas the Tri-DWT-based decomposed image is given to the deep learning model called CNN. Here, the optimization of hidden neurons in both NN and CNN is done by the improved meta-heuristic algorithm called FR-CSA for maximizing the detection accuracy. By using bit AND operator the results of both NN and CNN are combined for providing an improved classification accuracy for categorizing the image into normal and abnormal.

Image pre-processing

DE GRUYTER

In the image pre-processing, the green channel conversion, CLAHE and average filtering approaches are performed for improving the brightness of the image with less intensity variation among the pixels. Consider, B_{inp} as the input image.

Green channel conversion: To observe the abnormalities present in the image clearly, the input RGB image is converted into a green channel image. The image's contrast is enhanced using green channel conversion since the input retinal fundus images have very less contrast. Once the green channel conversion is done, the image representation is given by B_{green} .

CLAHE: It is employed to improve the image brightness. CLAHE is implemented as shown below.

- (1) Each input image is split into non-overlapping contextual regions of similar size including 8×8 blocks, each one is correlated with the neighborhood of 64 pixels.
- (2) Each contextual region's intensity histogram needs to be calculated.
- (3) For clipping the histograms, the clip limits are set. This is the threshold parameter for enhancing the image's contrast effectively. This requires to be set to the minimum optimal value.
- (4) Each histogram is modified by selecting the transformation functions.
- (5) By using the limit of constant clip limit, each histogram is modified and the corresponding equation is denoted in Eq. (1). Here, the calculated pixel value is denoted as p, the maximum and the minimum pixel values are given by p_{max} and p_{min} . The cumulative probability distribution is denoted as cmp(q).

$$p = [p_{\text{max}} - p_{\text{min}}] * \text{cmp}(q) + p_{\text{min}}$$
 (1)

In Eq. (2), the gray level is changed for performing exponential distribution. Here, the clip parameter is indicated by α . This approach functions on small sections of the image called "tiles" rather than the entire image. Thus, the histogram's output region is approximately similar to the histogram of each tile's brightness that is improved by considering the type of distribution.

$$p = p_{\min} - \left(\frac{1}{\alpha}\right) * \ln\left[1 - \exp\left(q\right)\right]$$
 (2)

(1) By using bilinear interpolation, the neighboring tiles are combined and the image's gray-scale values are modified for the enhanced histograms. The final CLAHE image is denoted as B_{clahe} , which is used for further processing.

Average filtering [26]: This process smooths the edges by minimizing the intensity among the neighborhood pixels. This is used for improving the target pixel and later the entire pixel's average is considered. The image's feature is helpful for viewing the size and shape of an image. The resultant image of CLAHE B_{clahe} , to this the average filtering is performed. The corresponding average filtering image is shown in Eq. (3).

$$B_{\text{avrg}} = \frac{1}{\text{avf}} \sum B_{\text{clahe}}(m, n)$$
 (3)

In the above equation, the order of the average filter is represented as avf. The pre-processed image B_{avrg} is applied for blood vessel segmentation for further processing.

Optimal binary thresholding-based blood vessel segmentation with feature extraction

Optimized blood vessel segmentation process

Here, the blood vessels are segmented by optimized binary thresholding, which considers the subtraction of CLAHE and average filtered image as input based on Eq. (4).

$$B_{\rm sub} = B_{\rm clahe} - B_{\rm avrg} \tag{4}$$

Image thresholding is applied to the subtracted image B_{sub} , which is a simple and efficient process for performing image partitioning into the foreground and background. This analysis is one type of image segmentation approach, which isolates the objects by converting the gray-scale images into binary images. By setting the thresholding value, Thresh, on the pixel intensity of the actual image, the binary image is obtained, and it is termed as thresholding. The binary thresholding equation is denoted in Eq. (5).

$$B_{\text{binary}}(m,n) = \begin{cases} 1 & \text{if } FI(m,n) > \text{ Thresh} \\ 0 & \text{if } FI(m,n) \le \text{ Thresh} \end{cases}$$
 (5)

In the above equation, the image intensity of the subtracted image is given by FI(m, n) and the threshold value, Thresh, is optimized by the developed FR-CSA algorithm. The bounding limit of the solution lies in between 0 and 1. The main objective of the optimized binary thresholdingbased segmentation is to maximize the segmentation accuracy for the ground truth image. Further, the segmented $B_{
m binary}$ undergoes area opening, which removes the linked components from the binary image based on "bwareaopen" function and the resultant image is given by $B_{
m open}$.

Feature extraction

In the proposed DR detection model, the features such as LBP and GLCM are extracted.

LBP [27]: In many of the applications from texture segmentation to detection, this model is quite appropriate. By thresholding, each neighborhood pixel, the LBP operator labels the image pixels and the output will be in form of binary format. The blood vessel segmented $B_{\rm open}$ is used as a descriptor, which is denoted in Eq. (6).

$$hst_{img} = \sum_{x,y} Ig(B_{open} = img), img = 0, \dots, m-1$$
 (6)

Here, the count of labels given by the LBP operator is given by m and Ig(D)=1 if D is true, whereas Ig(D)=0 if D is false. A uniformity measure um is defined in Eq. (7) by considering $lbp_{pb,rb}$ as pb-bit binary number $(e_{pb-1},e_{pb-2},\cdots,e_1e_0)$ for acquiring the rotation-invariant uniform pattern using finger angular quantization. The rotation invariant uniform pattern using um value less than or equal to two and it is determined in Eq. (8).

$$um(lbp_{pb,rb}) = |e_{pb-1} - e_0| + \sum_{pb=1}^{pb-1} |e_{pb} - e_{pb-1}|$$
 (7)

$$lbp_{pb,rb} = \begin{cases} \sum_{g=0}^{pb-1} C(gr_{pv} - gr_{cv}) & \text{if } um(lbp_{pb,rb}) \le 2 \end{cases}$$
 (8)

The gray value of the center pixel is denoted as gr_{pv} and the gray value of pb points is given by gr_{cv} and $g=0,\cdots$, pb-1. By selecting the circles with various radii around the center pixels, LBP is used for performing a multi-scale examination. Later, each scale creates a unique LBP image. LBP image's entropy and energy are constructed over a different number of pixels (pb=8, 16 and 24, and rb=1, 2 and 3, respectively) that are used as feature representations.

GLCM [28]: By considering the spatial relationship of pixels, GLCM is used for measuring the texture features. This method evaluates the probability of pixel pairs by having some specific values that are useful for examining the spatial relationship of an image. Eq. (9) denotes the mathematical formulation of energy.

$$eng = \sum_{u} \sum_{v} E_{uv}^2$$
 (9)

In the above equation, the $(u, v)^{th}$ element in the normalized GLCM is given by E_{uv} . The numerical equations

of entropy, homogeneity and contrast are expressed in Eq. (10), Eq. (11), and Eq. (12), correspondingly.

$$ent = -\sum_{u} \sum_{v} E_{uv} \log_2 E_{uv}$$
 (10)

hom =
$$\sum_{u} \sum_{v} \frac{1}{1 + (u - v)^2} E_{uv}$$
 (11)

$$con = \sum_{u,v} (u - v)^2 E_{uv}$$
 (12)

Based on Eq. (13), the variance is defined, in which the mean of E_{uv} is given by μ . "The mathematical formulations of sum average, and correlation are given in Eq. (14), and Eq. (15), respectively". Here, the count of gray level in the image is given by N_f . "The mean and standard deviation of E_x and E_y are indicated by (μ_x, μ_y) and (σ_x, σ_y) , respectively".

$$\operatorname{vrn} = \sum_{u} \sum_{v} (u - \mu)^2 E_{uv} \tag{13}$$

$$sav = \sum_{y=2}^{2N_f - 2} u E_{x+y}(u)$$
 (14)

$$crl = \frac{\sum_{u} \sum_{v} (u \times v) E_{uv} - \mu_{x} \mu_{y}}{\sigma_{x} \sigma_{v}}$$
 (15)

"The sum variance, difference variance, sum entropy, difference entropy, information measures of correlation (imc1, imc2) and maximum correlation coefficient" are denoted from Eq. (16) to Eq. (21), correspondingly. The term *LXY*, *LXY*1 and *LXY*2 are denoted in Eq. (22), Eq. (23) and Eq. (24), respectively. The Mathew's Correlation Coefficient is represented in Eq. (25).

$$svr = \sum_{u=2}^{2N_f} (u - sav)^2 E_{x+y}(u)$$
 (16)

$$dfv = Variance of E_{x-v}$$
 (17)

$$sent = \sum_{u=2}^{2N_f} E_{x+y}(u) \log\{E_{x+y}(u)\}$$
 (18)

$$dfe = \sum_{u=0}^{N_{f-1}} E_{x-y}(u) \log\{E_{x-y}(u)\}$$
 (19)

$$imc1 = \frac{LXY - LXY1}{\max\{LX, LY\}}$$
 (20)

$$imc2 = \sqrt{(1 - exp[-2.0[LXY2 - LXY]])}$$
 (21)

$$LXY = -\sum_{u} \sum_{v} E_{uv} \log_2 E_{uv}$$
 (22)

$$LXY1 = -\sum_{u} \sum_{v} E_{uv} \log_2 \{ E_x(u) E_y(v) \}$$
 (23)

$$LXY2 = -\sum_{u} \sum_{v} E_{x}(u) E_{y}(v) \log_{2} \{E_{x}(u) E_{y}(v)\}$$
 (24)

$$MCC = \sum_{w} \frac{E(u, w)E(v, w)}{E_{x}(u)E_{y}(w)}$$
 (25)

Therefore, the final LBP features are denoted as Fes_{lbp} and the GLCM features are represented as Fes_{glcm}. The final feature is attained by combining both LBP and GLCM features and it is indicated by Fes_n^{comb} , in which the term n = $1, 2, \dots, N$ and the whole count of features are given by N.

Image decomposition by Tri-Discrete Level **Decomposition**

By sending the image through the sequence of filters, DWT [29] of the image $B_{\rm open}$ is calculated. In order to obtain the result, the samples are sent through a low-pass filter with impulse response lpf and the corresponding equation is shown in Eq. (26).

$$J[n] = (B_{\text{open}} * \text{lpf})[n] = \sum_{H=-\infty}^{\infty} B_{\text{open}}[J] \text{lpf}[n-H]$$
 (26)

Consequently, the image is disintegrated using a highpass filter hpf. The result of the low-pass filter is subsampled and processed by transferring it again by a new 'high-pass filter and low-pass filter' by half the cut-off frequency of the final one. The mathematical formulations are denoted in Eq. (27) and Eq. (28).

$$J_{\text{low}}[n] = \sum_{H=-\infty}^{\infty} B_{\text{open}}[H] \text{lpf}[2n - H]$$
 (27)

$$J_{\text{high}}[n] = \sum_{H=-\infty}^{\infty} B_{\text{open}}[H] \text{hpf}[2n - H]$$
 (28)

Finally, the decomposed image is denoted as B^{dwt} and it is further subject to CNN for effective DR detection.

Fitness rate-based crow search algorithm for optimal blood vessel segmentation and detection

Conventional Crow Search Algorithm

The main inspiration of CSA [30] is the crow's behavior in search of food that was kept secretly by others in the secret locations. According to the body size of the crow, they have a huge brain. It mainly focuses on a group of intelligent crows. The task of the crows is observing the other crows for checking the secret place of food hidden by the other crows for robbing that food when the crows leave the place. The rules and regulations of CSA are given below.

- Crows are present in the bulk.
- The hidden places of food are memorized by the crows.

- To rob the food, crows follow each other.
- Crows protect their resources from looted.

Consider the dimensional space as Ds. which includes crow's position c at the time ts and it is defined by $P^{c,ts}(ps =$ 1, 2, ..., Nc; $ts = 1, 2, ..., ts_{max}$), where $P^{c, ts} = [P_1^{c, ts}, P_2^{c, ts},$ $\cdots, P_{DS}^{c,ts}$]. At ts_{max} maximum number of iterations, the total number of crows is Nc. The term $hd^{c,ts}$ denotes the location of the hidden crow, which is the best position of the crow. To observe the concealed position, the crow d is willing, which is denoted as $hd^{d,ts}$. The crow c plans to follow crow d, which moves toward the secret place of d. In this case, two conditions will be happened. The second crow doesn't have any idea that the first crow is following it, thus the new position of the crow c is acquired using Eq. (29).

$$P^{c,ts} = P^{c,ts} + \operatorname{rnd}_c \times Lf^{c,ts} \times (hd^{d,ts} - P^{c,ts})$$
 (29)

In the above equation, the random number that lies in between 0 and 1 is given by c, and the length of the flight of crow c at time ts is given by $Lf^{c,ts}$. The other condition is that the second crow will have the information that the first crow follows it, thus the second crow will fool it by moving to the false location. Eq. (30) represents the above two conditions, where the awareness probability of the crow d at the time ts is denoted as $Aw^{d,ts}$.

$$P^{c,ts} = \begin{cases} P^{c,ts} + \text{rnd}_c \times Lf^{c,ts} \times (hd^{d,ts} - P^{c,ts}) & \text{if } \text{rnd}_d \ge Aw^{d,ts} \\ \text{a random position} & \text{otherwise} \end{cases}$$
(30)

The CSA's step by step process is given as follows.

- (1) To tune the problem, the decision variables and conditions are employed. Next, the parameters of CSA are *Nc*, *ts*, *Lf* and *Aw* are evaluated.
- (2) The random positions of *Nc* crows in *Ds* dimensional search space. Eq. (31) represents each crow's feasible solution, in which the count of decision variables is denoted as dvr. In Eq. (32), the memory initialization is required for each crow since the crow doesn't have the information earlier.

$$\operatorname{Crs} = \begin{bmatrix} P_{1}^{1} & P_{2}^{1} & \cdots & P_{\operatorname{dyr}}^{1} \\ P_{1}^{2} & P_{2}^{2} & \cdots & P_{\operatorname{dyr}}^{2} \\ \vdots & \vdots & \vdots & \vdots \\ P_{1}^{Nc} & P_{2}^{Nc} & \cdots & P_{\operatorname{dyr}}^{Nc} \end{bmatrix}$$
(31)

$$Mm = \begin{bmatrix} hd_{1}^{1} & hd_{2}^{1} & \cdots & hd_{\text{dvr}}^{1} \\ hd_{1}^{2} & hd_{2}^{2} & \cdots & hd_{\text{dvr}}^{2} \\ \vdots & \vdots & \vdots & \vdots \\ hd_{1}^{Nc} & hd_{2}^{Nc} & \cdots & hd_{\text{dvr}}^{Nc} \end{bmatrix}$$
(32)

- (1) Each crow's position is defined effectively by specifying the decision variable values in the objective function.
- (2) In Eq. (29), crows create the position of new search space. To find the hidden food, the crow selects one from the cluster immediately.
- (3) The assessment of crow's new position feasibility is determined. The crow will update its location if it is perfect otherwise the crow will be in the current location itself.
- (4) Fitness function is defined for determining the new position of each crow.
- (5) In Eq. (33), the crow's memory is updated, where the objective function's value is expressed as $f(\cdot)$.

$$hd^{c,ts+1} = \begin{cases} P^{c,ts+1} & \text{if } f(P^{c,ts+1}) \text{is better than } f(hd^{c,ts}) \\ hd^{c,ts} & \text{otherwise} \end{cases}$$
(33)

By using the objective function value, the location of the best memory is linked and it is named as the optimal solution during termination. The pseudo-code representation of conventional CSA is shown in Algorithm 1.

```
Algorithm 1: Pseudocode of state-of-the-art CSA [30].
```

```
Initialization of the position of N_c crows is done Perform fitness evaluation
Perform the memory initialization
While ts < ts_{max}
For 1: N_c
Select the crow randomly from the search space Aw = 1
If rnd_d \ge P^{d,ts}
The position of each crow is calculated by Eq. (29) else
Choose a random location
End if
End for
Evaluation of the probability of new locations is done Compute the fitness values
Memory update is performed by Eq. (33)
End while
```

Proposed FR-CSA

The conventional CSA [30] is motivated from intelligent behavior of crows, which is a population-based approach. This is used for solving more optimization problems in engineering. CSA is having only a few parameters for adjusting and hence it is simple to implement. The major advantages of CSA are good convergence rate, and

produced competitive results. However, it can easily fall into local optima and lack of global optimization. For enhancing the performance of the conventional CSA, the fitness rate is considered in the proposed FR-CSA algorithm. Consider $\operatorname{ftn}(c)$ as the fitness of the current solution and the term mean (ftn) represents the average fitness value of the entire solution. If the term ($\operatorname{ftn}(c)$ < mean (ftn)), then the update process of proposed FR-CSA is shown in Eq. (34). Here, the fitness rate is denoted as ftnrt, the best fitness value is given by bestftn and the random number is indicated by rnd. The fitness rate is mathematically represented in Eq. (35), in which the mean of the fitness is indicated by mean (ftn) and the fitness value of crow c is given by $\operatorname{ftn}(c)$.

$$P^{c,ts^*} = P^{c,ts} + \text{ftnrt} \times \text{rnd} \left(\text{bestftn} - P^{c,ts} \right)$$
 (34)

$$ftnrt = \frac{bestftn - ftn(c)}{mean(ftn)}$$
(35)

In Algorithm 2, the step by step procedure of proposed FR-CSA is given.

Algorithm 2: Proposed FR-CSA

```
Initialization of the position of N_c crows is done
Perform fitness evaluation
Perform the memory initialization
While ts < ts_{max}
For 1: N_c
  Select the crow randomly from the search space
  Aw=1
    If rnd_d \ge P^{d, ts}
    The position of each crow is calculated by Eq. (29)
    Else if (ftn(c) < mean(ftn))
           The update process is done by the proposed
           model using Eq. (34)
    else
          The update process between upper and lower
           bound
           Choose a random location
    End if
  End for
Evaluation of the probability of new locations is done
Compute the fitness values
```

Optimized classification

End while

Memory update is performed by Eq. (33)

In the proposed DR detection model, the combination of NN and CNN are taken into consideration. The major



DE GRUYTER

Figure 2: Hidden neuron encoding of DR detection model.

contribution of the developed model is to optimize the number of hidden neurons in both NN and CNN, which is done by improved FR-CSA for maximizing the detection accuracy. The solution encoding of the hidden neuron optimization is shown in Figure 2. From Figure 2, the terms ne_{NN} and ne_{CNN} represent the count of hidden neurons of NN and CNN, respectively.

The objective function of the developed DR detection model is denoted in Eq. (36), and Eq. (37) represents the mathematical equation of detection accuracy.

$$Acc = \frac{Ps^{tr} + Ne^{tr}}{Ps^{tr} + Ne^{tr} + Ps^{fa} + Ne^{fa}}$$
(37)

In the above equation, "the true positives and true negatives are denoted as Ps^{tr} and Ne^{tr} , respectively. Moreover, the false positives and false negatives are indicated by Ps^{fa} and Ne^{fa} ".

Neural Network: The functionality of NN [31] is based on the neuron, which is an interconnected classifier that includes elements and nodes. The processing ability of the network is maintained in the interunit connection strength obtained using the adaption procedure, training pattern set. In NN, input a, hidden b, and output e layers are present. The structure of NN takes the features as input. The input features are represented as Fes_n^{comb} . The output layer of the hidden layer is calculated based on Eq. (38).

$$\overline{Q}^{(Q)} = \operatorname{Avf}\left(\tilde{B}_{(\widehat{A}b)}^{(Q)} + \sum_{a=1}^{IP(co)} \tilde{B}_{(ab)}^{Q} \operatorname{Fes}_{n}^{\operatorname{comb}}\right)$$
(38)

In Eq. (37), the count of input neurons is denoted as IP(co), the bias weight of *b*th neuron is given by $\tilde{B}_{(\widehat{A}b)}^{(Q)}$, the weight from *a*th neuron to *b*th be denoted as $\tilde{B}_{(ab)}^{Q}$, and the activation function is indicated by Avf. The total output of the network is denoted in Eq. (39).

$$\widehat{C}_e = \operatorname{Avf}\left(\widetilde{B}_{(\widehat{A}e)}^{(C)} + \sum_{b=1}^{OP(co)} \widetilde{B}_{(be)}^{(O)} \overline{Q}^{(Q)}\right)$$
(39)

In the above equation, the count of hidden neurons is represented as $OP(co) \leftarrow ne_{NN}$, the bias weight of $\tilde{B}_{(\widehat{A}e)}^{(C)}$ output neuron is indicated by $\tilde{B}_{(\widehat{Ae})}^{(C)}$, and the weight from bth neuron to eth neuron is expressed as $\tilde{B}_{(he)}^{(0)}$. The weight function of NN is given by $B_w^{NN} = \{\tilde{B}_{(\widehat{A}b)}^{(Q)}, \tilde{B}_{(\widehat{A}e)}^{(C)}, \tilde{B}_{(ab)}^{Q}, \tilde{B}_{(be)}^{(O)}\}$. For better training, the weight B_w^{NN} is optimally chosen based on Eq. (40).

arg min
$$ME = \left\{ \tilde{B}_{(\widehat{A}b)}^{(0)}, \tilde{B}_{(\widehat{A}e)}^{(C)}, \tilde{B}_{(ab)}^{Q}, \tilde{B}_{(be)}^{(0)} \right\} \sum_{e=1}^{C(co)} |C_e - \widehat{C}_e|$$
(40)

In the above equation, the forecasted value is given by \hat{C}_e and the actual value is represented as C_e .

Convolutional Neural Network: CNN [32] is an MLP, which is a special design for recognizing 2D-image. It has many layers, which include the "input layer, convolution layer, sample layer and output layer". Moreover, the structure of the deep networks has a sample layer and convolution layer, which have multiple. CNN doesn't restrict like the Boltzmann machine that requires being before and after the neuron layers in the next layer for all the connections, CNN algorithms, every neuron doesn't require a global image. By using Deep CNN, the extracted features are given as input. CNN is the feed forward NN's, where the data flows from one direction only. The input image is directly transferred to the network, which is usually seen in several convolutions and pooling layers phases. Thus, the last fully connected layer results in the class labels. In earlier, several changes are recommended in the architecture to improve the classification accuracy.

Convolutional Layer: The convolution layer acts as a feature extractor, which assess the input image's descriptor. In the convolutional layer, the neurons are considered as feature maps. To compute the feature map, inputs and weights are combined that are learned before and the convolved outputs are sent through a non-linear activation function. Though, various feature maps existing in the same layer will have discrete weights, thus from each region, multiple features need to be extracted. The dth output feature map A_d and it is computed using Eq. (41).

$$A_d = f(\operatorname{ftm}_d * B^{\operatorname{dwt}}) \tag{41}$$

In the above equation, the "convolutional filter linked with dth feature map is represented as ftm_d and the Tri-DWT image is considered as the input image and it is denoted as B^{dwt} , and the 2D Convolutional operator is denoted as *, and it is employed for computing filter's inner product in each region of the input image, and the nonlinear activation function is given by f(.)".

Pooling Layers: The spatial resolution of the feature map is the major intuition of the pooling layer. With this, the spatial invariance for translations and input distortions

has been obtained. With the help of pooling aggregation layers, the average of all input values of a very small image is transferred to the next layer. Each resultant map combines the convolution with many input maps. This pooling layer equation is denoted in Eq. (42).

$$A_d^{pl} = f\left(\sum_{i \in B_j} A_d^{pl-1} * k r_{ij}^{pl} + b s_j^{pl}\right)$$
 (42)

In Eq. (10), the pooling layer is denoted as pl, "the downsampling layer is indicated by pl-1, the input features of pl-1 convolutional layer is denoted as A^{pl-1} , the kernel maps of pl Convolutional layer is indicated by kr_{ij}^{pl} , and the additive bias of pl Convolutional layer is represented as bs_j^{pl} ", and the selection of input maps is given by B_j . The input and output are represented as i, j, respectively. In each respective field, max-pooling selects the principal element.

Fully connected layers: It is the final phase of CNN that includes a generic multi-layer network. Some of the last layers are fully connected to its 1D layers to all the activations present in the earlier layer. It is very easy for feature extraction from these layers to train the other classifier.

Training: In general, both NN and CNNs employ learning models for regulating the appropriate parameters for attaining the required network result. For specific use, backpropagation is the frequently used algorithm.

Thus, the optimized hybrid classification categorizes the input image into normal and abnormal.

Results and discussions

Experimental setup

The proposed DR detection model was implemented in MATLAB 2018a, and the analysis was done. The parameters have been tuned by the trial and error method, which is a fundamental method of problem solving. It is characterized by repeated, varied attempts, which are continued until success. The datasets used for the experiment was HRF, Messidor and DIARETDB. For analysis, the population size was considered as 10, and the maximum number of iterations was considered as 25. To detect DR, the proposed FR-CSA was compared over heuristic algorithms named PSO-NN+CNN [33], **GWO-NN+CNN** [34], WOA-NN+CNN [35], CSA-NN+CNN [26], FR-CSA-NN+CNN, whereas the analysis was compared over KNN [36], SVM [37], NN [31], CNN [32] and NN+CNN [31, 32] concerning the performance measures such as "accuracy,

sensitivity, specificity, precision, FPR, FNR, NPV, FDR, F1-score and MCC".

Evaluation metrics

The performance metrics that are considered for the experiment are given below.

- (a) Accuracy: The formula for accuracy is shown in Eq. (37).
- (b) Sensitivity: "the number of true positives, which are recognized exactly".

Sensitivity =
$$\frac{Ps^{tr}}{Ps^{tr} + Ne^{fa}}$$
 (43)

(c) Specificity: "the number of true negatives, which are determined precisely".

Specificity =
$$\frac{Ne^{tr}}{P_{S}fa}$$
 (44)

(d) Precision: "the ratio of positive observations that are predicted exactly to the total number of observations that are positively predicted".

$$Precision = \frac{Ps^{tr}}{Ps^{tr} + Ps^{fa}}$$
 (45)

(e) FPR: "the ratio of the count of false-positive predictions to the entire count of negative predictions".

$$FPR = \frac{Ps^{fa}}{Ps^{fa} + Ne^{tr}}$$
 (46)

(f) FNR: "the proportion of positives which yield negative test outcomes with the test".

$$FNR = \frac{Ne^{fa}}{Ne^{fa} + Ps^{tr}}$$
 (47)

(g) NPV: "probability that subjects with a negative screening test truly don't have the disease".

$$NPV = \frac{Ne^{fa}}{Ne^{fa} + Ps^{fa}}$$
 (48)

(h) FDR: "the number of false positives in all of the rejected hypotheses".

$$FDR = \frac{Ps^{fa}}{Ps^{fa} + Ps^{tr}} \tag{49}$$

(i) F1 score: "harmonic mean between precision and recall. It is used as a statistical measure to rate performance".

$$F1score = \frac{Sensitivity \bullet Precision}{Precision + Sensitivity}$$
(50)

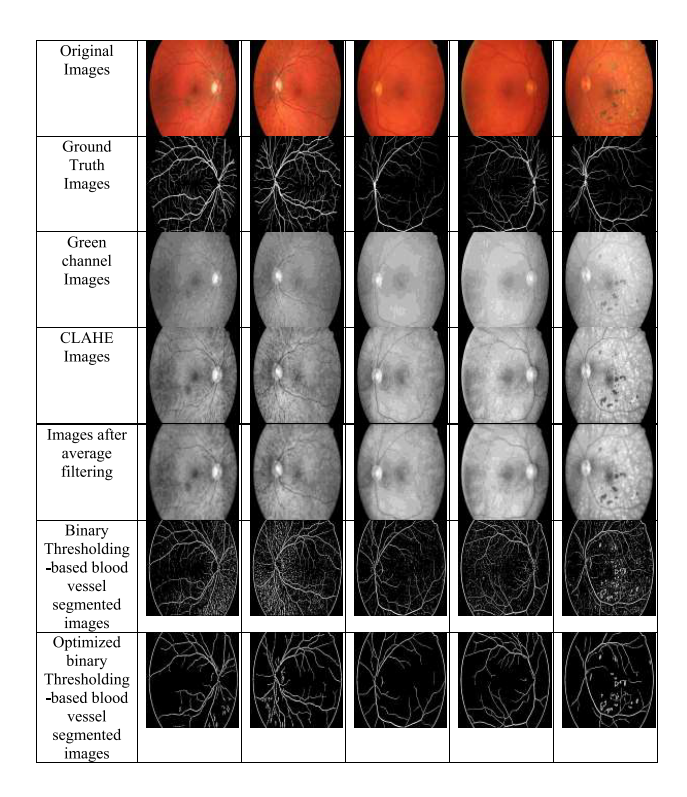


Figure 3: Experimental results of pre-processing, and segmentation.

MCC: It is a "correlation coefficient computed by four values".

$$MCC = \frac{Ps^{tr} \times Ne^{tr} - Ps^{fa} \times Ne^{fa}}{\sqrt{(Ps^{tr} + Ps^{fa})(Ps^{tr} + Ne^{fa})(Ne^{tr} + Ps^{fa})(Ne^{tr} + Ne^{fa})}}$$
(51)

Image results

Here, the results of green-channel images, CLAHE images, filtered images, binary thresholding and optimized binary thresholding-based blood vessel segmented images are given in Figure 3.

Performance analysis

The analysis on accuracy of the proposed FR-CSA-NN+CNN and the traditional heuristic algorithms for DR detection is shown in Figure 4 for the HRF image dataset, Messidor dataset, and DIARETDB dataset. In Figure 4 (A), the accuracy for the HRF dataset of the introduced FR-CSA-NN+CNN is 11.1% superior to PSO-NN+CNN, 25% superior to WOA-NN+CNN and 33.3% superior to FR-CSA-NN+CNN at learning percentage 35. When considering at all learning percentages, the accuracy of the improved CSA-NN+CNN is attaining the best performance. At learning percentage 75, the accuracy of the implemented FR-CSA-NN+CNN from Figure 4 (C) is 4.3% advanced than GWO-NN+CNN, 17.2% advanced than PSO-NN+CNN, and 31.9% advanced than CSA-NN+CNN. Figure 5 shows the overall performance analysis of the accuracy of the proposed FR-CSA-NN+CNN and the traditional machine learning algorithms concerning learning percentages for all three datasets. In Figure 5 (B), the accuracy of the implemented FR-CSA-NN+CNN at 35 learning percentage is 4.1% improved than NN+CNN, 40.8% improved than SVM, 2.8% improved than CNN, 44.9% improved than NN, and 53.8% improved than KNN.

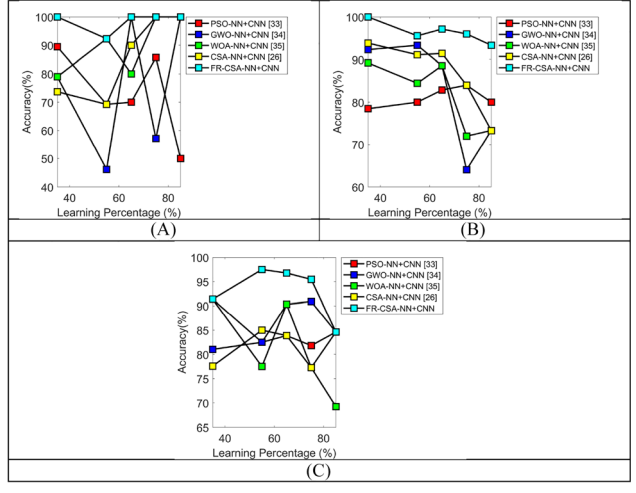


Figure 4: Analysis of heuristic algorithms for DR detection concerning the performance measure accuracy for (A) HRF dataset, (B) Messidor dataset, and (C) DIARETDB dataset.

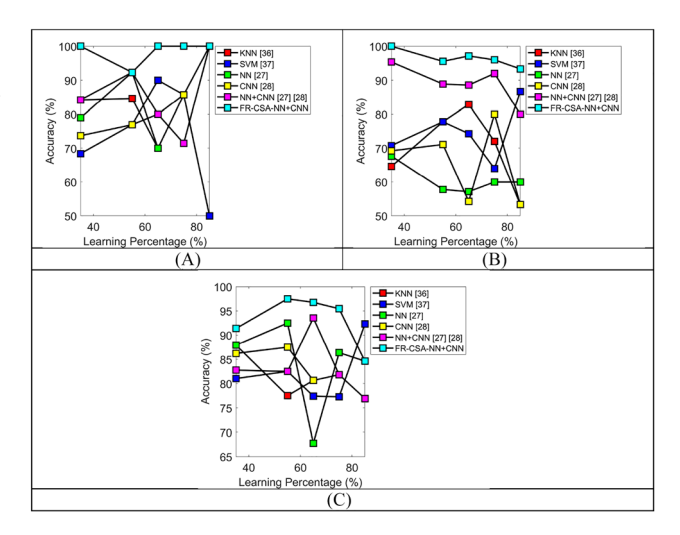


Figure 5: Analysis of machine algorithms for DR detection concerning the performance measure accuracy for (A) HRF dataset. (B) Messidor dataset, and (C) DIARETDB dataset.

Moreover, the accuracy of the suggested FR-CSA-NN+CNN from Figure 5 (A) is 17.6% advanced than SVM, 25% advanced than NN, 36.9% advanced than CNN, and 44.9% advanced than SVM at learning percentage 35. Thus, the results have shown that the implemented FR-CSA-NN+CNN is attaining the best results when compared over conventional algorithms for detecting DR effectively.

Overall performance analysis on HRF dataset

The overall performance analysis of the developed FR-CSA-NN+CNN and the conventional heuristic techniques on the HRF image dataset is shown in Table 2. In Table 2, the accuracy of the introduced FR-CSA-NN+CNN is producing the best outcomes when compared to existing algorithms. It is 33.1% progressed than PSO-NN+CNN and CSA-NN+CNN, 100% progressed than GWO-NN+CNN. Moreover, the precision of the implemented FR-CSA-NN+CNN is 25% surpassed than PSO and WOA-based NN+CNN, 60% surpassed than GWO-NN+CNN, and 66.6% surpassed than CSA-NN+CNN. In Table 3, the accuracy of the introduced FR-CSA and conventional machine learning algorithms is shown. It is 9%

progressed than KNN, 20% progressed than SVM and CNN. Therefore, it is confirmed that the developed FR-CSA-NN+CNN is achieving the best outcomes for DR detection.

Overall performance analysis on messidor dataset

The performance analysis on the Messidor dataset of the proposed and the conventional heuristic algorithms for performance measures is tabulated in Table 4. In Table 5, the overall analysis of the proposed and the conventional classifiers is shown. From Table 4, the accuracy of the improved FR-CSA-NN+CNN is 11.1% better than PSO-NN+CNN and CSA-NN+CNN, 45.8% better than GWO-NN+CNN, and 29.6% better than WOA-NN+CNN. Also, the precision of the developed FR-CSA-NN+CNN is acquiring the best results when compared over other algorithms. The precision of the suggested FR-CSA-NN+CNN is 25% improved than PSO-NN+CNN, 50% improved GWO-NN+CNN, and CSA-NN+CNN, and 12.4% improved than WOA-NN+CNN. From Table 5, the accuracy of the implemented FR-CSA-NN+CNN is 29.6% enhanced than KNN, 45.8% enhanced than SVM, 55.5% enhanced than NN,

Table 2: Overall performance analysis of heuristic algorithms for DR detection for HRF dataset.

"Performance measures"	PSO-NN+CNN [33]	GWO-NN+CNN [34]	WOA-NN+CNN [35]	CSA-NN+CNN [30]	FR-CSA-NN+CNN
"Accuracy"	0.69231	0.46154	0.92308	0.69231	0.92308
"Sensitivity"	0.57143	0.33333	1	0.6	0.83333
"Specificity"	0.83333	0.57143	0.88889	0.75	1
"Precision"	0.8	0.4	0.8	0.6	1
"FPR"	0.16667	0.42857	0.11111	0.25	0
"FNR"	0.42857	0.66667	0	0.4	0.16667
"NPV"	0.83333	0.57143	0.88889	0.75	1
"FDR"	0.2	0.6	0.2	0.4	0
"F1-score"	0.66667	0.36364	0.88889	0.6	0.90909
"MCC"	0.41476	-0.09759	0.84327	0.35	0.85391

Table 3: Overall performance analysis of machine learning algorithms for DR detection for HRF dataset.

"Performance measures"	KNN [36]	SVM [37]	NN [31]	CNN [32]	NN+CNN [31, 32]	FR-CSA-NN+CNN
"Accuracy"	0.84615	0.76923	0.92308	0.76923	0.92308	0.92308
"Sensitivity"	0.71429	0.625	0.83333	0.66667	0.83333	0.83333
"Specificity"	1	1	1	0.85714	1	1
"Precision"	1	1	1	0.8	1	1
"FPR"	0	0	0	0.14286	0	0
"FNR"	0.28571	0.375	0.16667	0.33333	0.16667	0.16667
"NPV"	1	1	1	0.85714	1	1
"FDR"	0	0	0	0.2	0	0
"F1-score"	0.83333	0.76923	0.90909	0.72727	0.90909	0.90909
"MCC"	0.73193	0.625	0.85391	0.53675	0.85391	0.85391

Table 4: Overall performance analysis of heuristic algorithms for DR detection for Messidor dataset.

"Performance measures"	PSO-NN+CNN [33]	GWO-NN+CNN [34]	WOA-NN+CNN [35]	CSA-NN+CNN [30]	FR-CSA-NN+CNN
"Accuracy"	0.84	0.64	0.72	0.84	0.93333
"Sensitivity"	0.6	0.33333	0.44444	0.75	1
"Specificity"	1	0.8125	0.875	0.85714	0.91667
"Precision"	1	0.5	0.66667	0.5	0.75
"FPR"	0	0.1875	0.125	0.14286	0.083333
"FNR"	0.4	0.66667	0.55556	0.25	0
"NPV"	1	0.8125	0.875	0.85714	0.91667
"FDR"	0	0.5	0.33333	0.5	0.25
"F1-score"	0.75	0.4	0.53333	0.6	0.85714
"MCC"	0.68825	0.1639	0.35902	0.52117	0.82916

Table 5: Overall performance analysis of machine learning algorithms for DR detection for Messidor dataset.

"Performance measures"	KNN [36]	SVM [37]	NN [31]	CNN [32]	NN+CNN [31, 32]	FR-CSA-NN+CNN
"Accuracy"	0.72	0.64	0.6	0.8	0.92	0.93333
"Sensitivity"	0.45455	0.36364	0.3	0.55556	1	1
"Specificity"	0.92857	0.85714	0.8	0.9375	0.90476	0.91667
"Precision"	0.83333	0.66667	0.5	0.83333	0.66667	0.75
"FPR"	0.071429	0.14286	0.2	0.0625	0.095238	0.083333
"FNR"	0.54545	0.63636	0.7	0.44444	0	0
"NPV"	0.92857	0.85714	0.8	0.9375	0.90476	0.91667
"FDR"	0.16667	0.33333	0.5	0.16667	0.33333	0.25
"F1-score"	0.58824	0.47059	0.375	0.66667	0.8	0.85714
"MCC"	0.44529	0.25661	0.11471	0.55415	0.77664	0.82916

Table 6: Overall performance analysis of heuristic algorithms for DR detection for DIARETDB dataset.

"Performance measures"	PSO-NN+CNN [33]	GWO-NN+CNN [34]	WOA-NN+CNN [35]	CSA-NN+CNN [30]	FR-CSA-NN+CNN
"Accuracy"	0.81818	0.90909	0.77273	0.77273	0.95455
"Sensitivity"	0.55556	1	0.5	0.5	0.83333
"Specificity"	1	0.89474	0.8	0.875	1
"Precision"	1	0.6	0.2	0.6	1
"FPR"	0	0.10526	0.2	0.125	0
"FNR"	0.44444	0	0.5	0.5	0.16667
"NPV"	1	0.89474	0.8	0.875	1
"FDR"	0	0.4	0.8	0.4	0
"F1-score"	0.71429	0.75	0.28571	0.54545	0.90909
"MCC"	0.65179	0.7327	0.2058	0.39853	0.88561

16.6% enhanced than CNN, and 1.4% enhanced than NN+CNN. Hence, it is concluded that the recommended FR-CSA-NN+CNN is superior to conventional algorithms in attaining the best outcomes in detecting DR.

Overall performance analysis on DIARETDB dataset

For the DIARETDB dataset, the overall analysis of the developed FR-CSA-NN+CNN and the conventional

approaches is shown in Table 6, whereas Table 7 shows the comparison of the proposed FR-CSA-NN+CNN over machine learning algorithms. In Table 6, the accuracy of the recommended FR-CSA-NN+CNN is outperforming the conventional algorithms. It is 16.6% outperformed than PSO-NN+CNN, 5.0% outperformed than GWO-NN+CNN, outperformed than WOA-NN+CNN 23.5% CSA-NN+CNN. Moreover, the precision of the introduced FR-CSA-NN+CNN is 66.6% improved than GWO-NN+CNN CSA-NN+CNN, and 80% improved WOA-NN+CNN. From Table 7, the accuracy of the offered

Table 7: Overall	performance analy	vsis of machine I	learning algorithms	for DR detection	on for diaretdb dataset.

"Performance measures"	KNN [36]	SVM [37]	NN [31]	CNN [32]	NN+CNN [31, 32]	FR-CSA-NN+CNN
"Accuracy"	0.81818	0.77273	0.86364	0.81818	0.81818	0.95455
"Sensitivity"	0.57143	0.5	0.75	0.55556	0.55556	0.83333
"Specificity"	0.93333	0.92857	0.88889	1	1	1
"Precision"	0.8	0.8	0.6	1	1	1
"FPR"	0.066667	0.071429	0.11111	0	0	0
"FNR"	0.42857	0.5	0.25	0.44444	0.44444	0.16667
"NPV"	0.93333	0.92857	0.88889	1	1	1
"FDR"	0.2	0.2	0.4	0	0	0
"F1-score"	0.66667	0.61538	0.66667	0.71429	0.71429	0.90909
"MCC"	0.56101	0.49195	0.58801	0.65179	0.65179	0.88561

FR-CSA-NN+CNN is 16.6% superior to KNN, CNN and NN+CNN, 23.5% superior to SVM and 10.5% superior to NN. Thus, it is proved that the developed FR-CSA-NN+CNN are acquiring the best performance when compared over conventional algorithms for DR detection.

Conclusion

The present paper has introduced a new technique for effective DR detection by performing novel blood vessel segmentation and classification techniques. The input image was undergone pre-processing, where channel conversion, CLAHE, and average filtering techniques green were performed. Next, the blood vessel segmentation was done by the optimized binary thresholding approach. Later, Tri-DWT was done for decomposing the segmented image. From the segmented images, the features such as LBP and GLCM were extracted. These features were applied to NN, whereas the decomposed image was applied to CNN. Further, both the segmentation and classification phases were improved by the proposed FR-CSA algorithm by tuning the threshold and hidden neurons for accuracy maximization. The analysis has shown that the accuracy for the HRF dataset of the introduced FR-CSA-NN+CNN was 11.1% advanced than PSO-NN+CNN, 25% advanced than WOA-NN+CNN, and 33.3% advanced than CSA-NN+CNN at a learning percentage 35. Thus, it is confirmed that the developed FR-CSA algorithm has supported for best detection accuracy in diagnosing DR.

Research funding: None.

Author contributions: All the authors have accepted responsibility for the entire content of this submitted manuscript and approved submission.

Competing interests: The authors declare that they have no conflict of interest.

Ethical Approval: The conducted research is not related to either human or animal use.

References

- Zeng X, Chen H, Luo Y, Ye W. Automated diabetic retinopathy detection based on binocular siamese-like convolutional neural network. IEEE Access 2019;7:30744-53.
- Guariguata L, Whiting DR, Hambleton I, Beagley J, Linnenkamp U, Shaw JE. Global estimates of diabetes prevalence for 2013 and projections for 2035. Diabetes Res Clin Pract 2014;103: 137–49.
- Gargeya R, Leng T. Automated identication of diabetic retinopathy using deep learning. Ophthalmology 2017;124:962–9.
- 4. González-Gonzalo C, Sánchez-Gutiérrez V, Hernández-Martínez P, Contreras I, Lechanteur YT, Domanian A, et al. Evaluation of a deep learning system for the joint automated detection of diabetic retinopathy and age-related macular degeneration. Acta Ophthalmologica. Hoboken: Wiley; 2020, vol. 98:368–77.
- Quellec G, Charrière K, Boudi Y, Cochener B, Lamard M. Deep image mining for diabetic retinopathy screening. Med Image Anal 2017;39:178–93.
- Amin J, Sharif M, Yasmin M, Ali H, Fernandes SL. A method for the detection and classification of diabetic retinopathy using structural predictors of bright lesions. J Comput Sci 2017;19: 153-64
- Abràmoff MD, Lavin PT, Birch M, Shah N, Folk JC. Pivotal trial of an autonomous Al-based diagnostic system for detection of diabetic retinopathy in primary care. NPJ Digit Med 2018;1:39.
- Qummar S, Khan FG, Shah S, Khan A, Shamshirband S, Rehman ZU, et al. A deep learning ensemble approach for diabetic retinopathy detection. IEEE Access 2019;7:150530-9.
- He L, Li J, Plaza A, Li Y. Discriminative low-rank gabor filtering for spectral-spatial hyperspectral image classification. IEEE Trans Geosci Rem Sens 2017;55:1381–95.
- Hameed MA, Hassaballah M, Aly S, Awad AI. An adaptive image steganography method based on histogram of oriented gradient and PVD-LSB techniques. IEEE Access 2019;7:185189–204.
- 11. Guo Z, Wang X, Zhou J, You J. Robust texture image representation by scale selective local binary patterns. IEEE Trans Image Process 2016;25:687–99.
- Xiang Y, Wang F, You H. OS-SIFT: A robust SIFT-like algorithm for high-resolution optical-to-SAR image registration in suburban areas. IEEE Trans Geosci Rem Sens 2018;56:3078–90.
- 13. Mateen M, Wen J, Hassan M, Nasrullah N, Sun S, Hayat S. Automatic detection of diabetic retinopathy: a review on datasets, methods and evaluation metrics. IEEE Access 2020;8:48784–811.

- 14. Dutta S, Manideep BC, Basha SM, Caytiles RD, Ivengar NC. Classification of diabetic retinopathy images by using deep learning models. Int J Grid Distrib Comput 2018; 11:89-106.
- 15. Nida N, Irtaza A, Javed A, Yousaf MH, Mahmood MT. Melanoma lesion detection and segmentation using deep region based convolutional neural network and fuzzy c-means clustering. Int J Med Inform 2019:124:37-48.
- 16. Flaxman SR, Bourne RR, Resnikoff S, Ackland P, Braithwaite T, Cicinelli MV, et al. Global causes of blindness and distance vision impairment 1990-2020: a systematic review and meta-analysis. Lancet Glob Health 2017;5:e1221-34.
- 17. Quellec G, Lamard M, Erginay A, Chabouis A, Massin P, Cochener B, et al. Automatic detection of referral patients due to retinal pathologies through data mining. Med Image Anal 2016;29:47-64.
- 18. Dietterich TG, Lathrop RH, Lozano-Pérez T. Solving the multiple instance problem with axis-parallel rectangles. Artif Intell 1997; 89:31-71.
- 19. Quellec G, Lamard M, Abràmoff M.D. A multiple-instance learning framework for diabetic retinopathy screening. Med Image Anal 2012;16:1228-40.
- 20. Costa P, Galdran A, Smailagic A, Campilho A. A weaklysupervised framework for interpretable diabetic retinopathy detection on retinal images. IEEE Access 2018;6:18747-58.
- 21. Kar SS, Maity SP. Automatic detection of retinal lesions for screening of diabetic retinopathy. IEEE (Inst Electr Electron Eng) Trans Biomed Eng 2018;65:608-18.
- 22. Zhou L, Zhao Y, Yang J, Yu Q, Xu X. Deep multiple instance learning for automatic detection of diabetic retinopathy in retinal images. IET Image Process 2018;12:563-71.
- 23. Amin J, Sharif M, Rehman A, Raza M, Mufti MR. Diabetic retinopathy detection and classification using hybrid feature set, Special Section. Light Sheet Fluoresc Illum Microsc 2018;81:990-6.
- 24. Xu J, Zhang X, Chen H, Li J, Zhang J, Shao L, et al. Automatic analysis of microaneurysms turnover to diagnose the progression of diabetic retinopathy. IEEE Access 2018;6: 9632-42.
- 25. Roshini TV, Ravi RV, Mathew AR, Kadan AB, Subbian PS. Automatic diagnosis of diabetic retinopathy with the aid of

- adaptive average filtering with optimized deep convolutional neural network. Int J Imag Syst Technol 2020;30:1173-93.
- 26. Nosrati M, Karimi R. Detection of circular shapes from impulse noisy images using median and laplacian filter and Circular Hough Transform. In: 2011 8th International Conference on Electrical Engineering, Computing Science and Automatic Control. IEEE: Merida City; 2011:1-5 p.
- 27. Liao S, Law MWK, Chung ACS. Dominant local binary patterns for texture classification. IEEE Trans Image Process 2009;18: 1107-18.
- 28. Malegori C, Franzetti L, Guidetti R, Casiraghi E, Rossi R. GLCM, an image analysis technique for early detection of biofilm. J Food Eng
- 29. Tabassum F, Islam I, Amin MR. Comparison of filter banks of DWT in recovery of image using one dimensional signal vector. I King Saud Univ Comput Inform Sci 2019;1-10. https://doi.org/10. 1016/j.jksuci.2019.03.005.
- 30. Askarzadeh A. A novel metaheuristic method for solving constrained engineering optimization problems: crow search algorithm. Comput Struct 2016;169:1-12.
- 31. Fernández-Navarro F, Carbonero-Ruz M, Alonso DB, Torres-Jiménez M. Global sensitivity estimates for neural network classifiers. IEEE Trans Neural Netw Learn Syst 2017;28: 2592-604.
- 32. Namatēvs I. Deep convolutional neural networks: structure, feature extraction and training. Inf Technol Manag Sci 2017;20:
- 33. Pedersen MEH, Chipperfield AJ. Simplifying particle swarm optimization. Appl Soft Comput 2010;10:618-28.
- 34. Mirjalili S, Mirjalili SM, Lewis A. Grey wolf optimizer. Adv Eng Software 2014;69:46-61.
- 35. Mirjalili S, Lewis A. The whale optimization algorithm. Adv Eng Software 2016;95:51-67.
- 36. Chen Y, Hu X, Fan W, Shen L, Zhang Z, Liu X, et al. Fast density peak clustering for large scale data based on KNN. Knowl Base Syst 2019;187:1-7.
- 37. Yu S, Tan KK, Sng BL, Shengjin, Sia ATH. Lumbar ultrasound image feature extraction and classification with support vector machine. Ultrasound Med Biol 2015;41:2677-89.